Mon. Not. R. Astron. Soc. **000**, 1–?? (2015) Printed 24 November 2015 (MN LATEX style file v2.2)

Synchrotron emission in GRBs observed by Fermi: Its limitations and the role of the photosphere.

S. Iyyani[1,2,3,4⋆], F. Ryde[1,2], J.M. Burgess[1,2], A. Pe'er[5], D. Bégué[1,2]
[1] *Department of Physics, KTH Royal Institute of Technology, AlbaNova, SE-106 91 Stockholm, Sweden*
[2] *The Oskar Klein Centre for Cosmoparticle Physics, AlbaNova, SE-106 91 Stockholm, Sweden*
[3] *Department of Physics, Stockholm University, AlbaNova, SE-106 91 Stockholm, Sweden*
[4] *Erasmus Mundus Joint Doctorate in Relativistic Astrophysics*
[5] *Department of Physics, University Cork, 5 Brighton Villas, Western Road, Cork, Ireland*

arXiv:1511.07390v1 [astro-ph.HE] 23 Nov 2015

Accepted... Received...; in original form ...

ABSTRACT

It has been suggested that the prompt emission in gamma-ray bursts consists of several components giving rise to the observed spectral shape. Here we examine a sample of the 8 brightest, single pulsed *Fermi* bursts whose spectra are modelled by using synchrotron emission as one of the components. Five of these bursts require an additional photospheric component (blackbody). In particular, we investigate the inferred properties of the jet and the physical requirements set by the observed components for these five bursts, in the context of a baryonic dominated outflow, motivated by the strong photospheric component. We find similar jet properties for all five bursts: the bulk Lorentz factor decreases monotonously over the pulses and lies between 1000 and 100. This evolution is robust and can neither be explained by a varying radiative efficiency nor a varying magnetisation of the jet assuming the photosphere radius is above the coasting radius). Such a behaviour challenges several dissipation mechanisms, e.g., the internal shocks. Furthermore, in all 8 cases the data clearly reject a fast-cooled synchrotron spectrum (in which a significant fraction of the emitting electrons have cooled to energies below the minimum injection energy), inferring a typical electron Lorentz factor of $10^4 - 10^7$. Such values are much higher than what is typically expected in internal shocks. Therefore, while the synchrotron scenario is not rejected by the data, the interpretation does present several limitations that need to be addressed. Finally, we point out and discuss alternative interpretations.

Key words: gamma-ray bursts – photosphere

1 INTRODUCTION

Since gamma-ray burst (GRB) spectra mostly have a non-thermal shape, an early suggestion for the emission mechanism was optically-thin synchrotron emission (Katz 1994; Tavani 1996; Rees & Mészáros 1994; Sari et al. 1998). The viability of this model has been mainly ascertained by studying the low-energy photon index, α, of the Band function fits (e.g. Preece et al. (1998); Goldstein et al. (2013)). A large fraction of bursts have an $\alpha > -2/3$ which is incompatible with the simplest models of synchrotron emission. In addition to this, Axelsson & Borgonovo (2015) and Yu et al. (2015) studied the width of the νF_ν spectrum and found that a majority of long GRBs are too narrow to be explained by synchrotron emission, even from the most narrow electron distributions. The bursts with the narrowest spectra are even consistent with a single Planck function through out the burst duration (Ryde 2004; Ghirlanda et al. 2013; Larsson et al. 2015).

A possible explanation to these observations was given by the two-emission–zone model, which combines photospheric emission (quasi-Planck spectrum) with a non-thermal component (Mészáros & Rees 2000; Mészáros et al. 2002). The latter component is expected to be emitted from dissipation events in the optically-thin region of the flow. Indeed, fits with a blackbody in combination with a non-thermal component did perform well in many bursts (Ryde 2005; Ryde & Pe'er 2009; Guiriec et al. 2011; Axelsson et al. 2012; Iyyani et al. 2013). In these fits the non-thermal emission was modelled either by a power-law or a Band function.

⋆ email: shabuiyyani@particle.kth.se

© 2015 RAS

However, these are empirical functions and do not incorporate the actual emission physics. Therefore, they can, at best, only model the shape of physical spectra over a limited energy range.

Initial steps fitting physical models using proper spectral deconvolution were made by Liang et al. (1983) and Tavani (1996). Similarly, Burgess et al. (2014) studied the GRB spectra of a sample of the 8 brightest single-pulsed bursts by fitting a blackbody + synchrotron emission model. In these fits, the synchrotron component was calculated assuming a prescribed electron energy distribution. A significant blackbody component was identified in 5 of these bursts. For three of the eight bursts synchrotron emission alone is consistent with the data. However, for all cases a fast-cooling synchrotron emission is much too broad and is strongly contradicted by the data. Such spectra are expected when the cooling is complete and the electrons radiate most of their energy. The synchrotron emission that is permitted by the data indicate that a majority of electrons, at the minimum injection energy, have not had time to cool significantly. In other words, such emission can be denoted as incompletely cooled synchrotron emission, since it could be due to one of several reasons: first, the electrons might not have had time to loose most of their energy (so called slow-cooling; Sari et al. (1998); Asano & Terasawa (2009); Zhang & Yan (2011)), second, reheating of the electrons can compensate for the cooling (Kumar & McMahon 2008; Beniamini & Piran 2014), third, the electrons might be in a moderately fast cooling regime as described in Uhm & Zhang (2014). In such a model while the electrons are in the fast cooling regime, $t_{\rm cool} <\sim t_{\rm dyn}$ and therefore the emergent spectrum is intermediate between slow and fast cooling, and fourth, if the emission region has a varying magnetic field, only a fraction of the electrons will be able to cool efficiently, leaving a predominantly uncooled electron distribution (Pe'er & Zhang 2006; Beniamini & Piran 2014; Zhang et al. 2015).

In the current paper, we use the identified photospheric component of the five bursts to determine the properties of the flow at the photosphere (assuming it to be baryonic-dominated), such as Lorentz factor, Γ, photospheric radius, $r_{\rm ph}$, nozzle radius, r_0 and saturation radius, r_s (§2). Assuming that these properties are the same at the optically-thin emission site we study the synchrotron component to constrain the magnetic field strength, B and the electron Lorentz factor, $\gamma_{\rm el}$ at the dissipation site (§3). In §4 we investigate how and if a varying radiative efficiency or magnetisation can influence the determined parameter evolutions. We discuss the limitations of the presented interpretation in §5 and finally conclude in §6.

1.1 Sample and spectral properties

The eight bursts in the sample were selected by requiring that peak flux should be greater than 5 photons $\rm s^{-1}\,cm^{-2}$ in the energy range 10 keV to 40 MeV and that the light curves of the bursts should be single-peaked, in order to avoid overlap with different emission episodes. The bursts were binned following the Bayesian-block method (Scargle et al. 2013), which ensures that the binning is mainly determined by significant changes in the count rate. The following bursts were found to have a significant and strong blackbody component: GRB081224A (Wilson-Hodge et al. 2008), GRB090719A (van der Horst 2009), GRB100707A (Wilson-Hodge & Foley 2010), GRB110920A (McGlynn et al. 2012; Iyyani et al. 2015; Shenoy et al. 2013), weak but statistically significant: GRB110721A (Tierney & von Kienlin 2011), while GRB081110A, GRB090809A and GRB110407A were found to be consistent with a synchrotron component alone.

Burgess et al. (2014) found that the blackbody temperature decreases as a broken power-law and that the normalisation of the blackbody increases linearly with time for all bursts. These results are in agreement with the observations previously made by Ryde (2005); Ryde & Pe'er (2009); Axelsson et al. (2012). The spectral peak of the synchrotron emission, $E_{\rm sync}$, was found to decrease from hard to soft, as a broken power-law, for all the bursts.

2 THE PHOTOSPHERE COMPONENT AND THE DETERMINATION OF THE FLOW PROPERTIES

The detection of a strong blackbody component suggests that the flow is baryonic dominated as opposed to Poynting flux dominated, that is, the acceleration is predominantly done by the thermal pressure. This is because for Poynting flux dominated outflows, using the standard assumption of constant reconnection rate (Drenkhahn & Spruit 2002) the photospheric component is expected to be suppressed (Zhang & Pe'er 2009; Hascoët et al. 2013) and have a peak energy larger than a few MeV (Bégué & Pe'er 2015). This is in contrast to the strong thermal components observed at $\sim$ 100 keV in the 5 bursts studied here, which initially lie at around 40% (see §2.3), apart from GRB110721A which only has a few per cent blackbody flux. We point out that GRB110721A has been interpreted within a Poynting flux dominated model as well (Gao & Zhang 2015), and it is possible that the magnetisation is non-negligible, though weaker, in the other bursts, where the thermal component is more pronounced.

In this section, we consider the baryonic scenario in which the photosphere is formed at a radius above the saturation radius following the standard (non-dissipative) fireball evolution (Mészáros 2006). The flow is imagined to be advected through the photosphere, whose position is determined by the properties set by the central engine. The variability timescales observed for the bursts (on the order of the pulse width, $t_{\rm pulse}$) are much longer than both the dynamical timescales and the typical widths of the time-bins used in the analysis. The former is the time the flow takes to reach the photosphere, $t_{\rm dyn} \equiv r_{\rm ph}/2\Gamma^2 c = 0.2$ ms, where $r_{\rm ph} = 10^{12}$ cm, $\Gamma = 300$ is assumed and c is the speed of light. Therefore, it is safe to assume that the central engine is approximately steady and thereby the flow is quasi-static over the duration of each time-bin.

At some radius above the photosphere a fraction of the kinetic energy of the outflow is dissipated by some unspecified mechanism, accelerating the electrons to high energies. The likely distribution that is expected from diffusive shocks is a Maxwellian - Boltzmann distribution with an extension of a power-law at high energies (Baring et al. 1995; Spitkovsky 2008). Such an electron distribution is, indeed, consistent with the distribution required by the synchrotron fits done to the data (Tavani 1996; Burgess et al. 2014).

For each time bin, we estimate the outflow parameters Γ, $r_{\rm ph}$, r_0 and $r_{\rm s}$ by using the methodology described in Pe'er et al. (2007): we use the blackbody's temperature, T, its normalisation, which is parameterised by,

$$\mathcal{R} = \left(\frac{F_{\rm BB}}{\sigma_{\rm SB} T^4}\right)^{1/2} = \phi \frac{(1+z)^2}{d_L} \frac{r_{\rm ph}}{\Gamma}, \quad (1)$$

where $\sigma_{\rm SB}$ is Stefan-Boltzmann constant and ϕ is a factor of the order of unity (Pe'er et al. 2007), d_L is the luminosity distance and F is the total observed flux. We assume a redshift of $z = 2$, the average value for GRBs (Bagoly et al. 2006), and assume a flat universe ($\Omega_\Lambda = 0.73, H_0 = 71$ km/s/Mpc). The estimated outflow parameters change within a factor of a few for a different value of z, however, the time evolution of the behaviour of the parameters remain the same, see Iyyani et al. (2013).

We point out that we interpret the evolution of the flux and temperature as being due to central engine variations which causes evolution in the parameters. Alternative explanations involving high-latitude emission are discussed in Pe'er (2008); Pe'er & Ryde (2011), and Lundman et al. (2013).

2.1 Lorentz factor

The Lorentz factor is found to decrease monotonously with time in the 5 bursts which have a significant photospheric component, as shown in Figure 1. The Lorentz factor is derived from the observables by

$$\Gamma \propto (F/\mathcal{R})^{1/4} Y^{1/4} \quad (2)$$

where Y relates to the radiative efficiency of the burst which is given by

$$Y = \frac{L_0}{L_{\rm obs,\gamma}} \quad (3)$$

where L_0 is the total kinetic luminosity and $L_{\rm obs,\gamma}$ is the observed $\gamma-$ray luminosity. Since during the rise phase of the pulse, both the total flux and $\mathcal{R}$ increase with nearly a similar rate, the Lorentz factor remains close to a constant or sometimes shows only a moderate decrease with time. However, during the decay phase Γ decreases much faster, since $\mathcal{R}$ continues to increase while the flux decreases.

The upper left-hand panel in Figure 2 shows the range over which the Lorentz factor varies. All deduced values lie above 100 and only one burst (GRB100707A) has an initial value of Γ greater than 1000. The average value of Γ for the sample, considering their temporal evolution, is $\langle\Gamma\rangle = 377 \pm 205$.

2.2 Photospheric radius

The photosphere is the deepest region in the outflow from where photons can be observed. The derived values of the photospheric radius, $r_{\rm ph}$, is found to vary moderately with time (within a factor of ten), see Figure 3. The average value of $r_{\rm ph}$ for these bursts is $\langle r_{\rm ph}\rangle = 10^{11.8\pm0.4}$ cm, and the deduced ranges of values for different bursts are shown in the upper right-hand panel in Figure 2.

The dependance of $r_{\rm ph}$ on the observables is given by

$$r_{\rm ph} \propto L_0/\Gamma^3 \propto \dot{M}/\Gamma^2 \quad (4)$$

where $\dot{M}$ is the baryon load and is given by $\dot{M} = L_0/\Gamma c^2$. The evolution of the photospheric radius thus depends on a combination of the evolution in baryon load and Lorentz factor: the increase in baryon load increases the particle density, whereas the Lorentz factor effects the optical depth through $\tau = (n_e \sigma_T R)/2\Gamma^2$, where n_e is the electron number density at R, which is the distance of the emission site from the central engine, and σ_T is the Thompson cross-section. In particular, the evolution of $r_{\rm ph}$ is very sensitive to the changes in Γ.

During the rise phase of the pulse, the variation in $r_{\rm ph}$ is mainly given by the variation in the luminosity of the burst, since $\Gamma \sim$ constant (§2.1). This corresponds to an increase of the baryon load which causes the opacity, due to the electrons associated with the baryons, to increase, thereby increasing the photosphere radius. However, since the luminosity of the burst shows a corresponding increase, the energy per baryon (i.e Γ) remains nearly constant during the rise phase of the GRB pulse.

On the other hand, during the decay phase of the pulse, both Γ and L_0 decrease, whereas $r_{\rm ph}$ is found to be nearly steady or moderately increasing. In order to keep $r_{\rm ph}$ steady, it requires that $L_0 \propto \Gamma^3$ (or $\dot{M} \propto \Gamma^2$).

2.3 Nozzle and saturation radii

The nozzle radius of the jet, r_0, signifies the radius from where the jet starts to accelerate[1]. The bursts show a common behaviour according to which r_0 initially increasing by a factor of approximately ten (Fig. 3). After a few seconds, r_0 decreases again reaching its original value. One exception is, however, GRB110920A for which the r_0–break occurs after 100 seconds. We note that maximal value of r_0 is not attained in coincidence with the peak of the light curve, but is attained during the decay phase (with the exception of GRB081224A where the r_0-peak occurs just before the light-curve peak.) The lower left-hand panel in Figure 2 shows that the observed value of r_0 varies within the range of 10^6 to a few $\times 10^9$ cm, with an average value, $r_{0,\rm av} = 10^{7.9\pm0.8}$ cm. These values are well within the expected range between the black hole event horizon radius [10^{6-7}cm for a black hole mass of $5 - 10\ M_\odot$ (Paczyński 1998)] and the size of the core of an expected progenitor Wolf-Rayet star (Woosley & Weaver 1995). This suggests that r_0 is related to the interaction between the jet and the progenitor star (Thompson et al. 2007; Iyyani et al. 2013) , see further discussion in section 5.3. Figure 4 shows the correlation between r_0 and Γ. The break in the correlation is mainly due to the break in the evolution of r_0 occurring during the pulse decay phase.

The pulse-like temporal behaviour in r_0 gets reflected in the behaviour of $r_{\rm s}$, see Figure 3. For the bursts in the sample, $r_{\rm s}$ has an average value $\langle r_s\rangle = 10^{10.5\pm0.8}$ cm. The ratio $r_{\rm s}/r_{\rm ph}$ also varies with time. This ratio is given by $(F_{\rm BB}/F_{\rm kin})^{3/2}$, where $F_{\rm BB}$ is the blackbody flux and $F_{\rm kin}$ is the kinetic energy flux at the photosphere (eq. 1 in Iyyani et al. (2013)). Figure 5 shows the ratio of the

[1] Note that the radius r_0 does not necessarily need to correspond to the radius of the central engine, and instead can be related to the dissipation pattern of the flow within the star (Thompson et al. 2007; Iyyani et al. 2013; Pe'er et al. 2015).

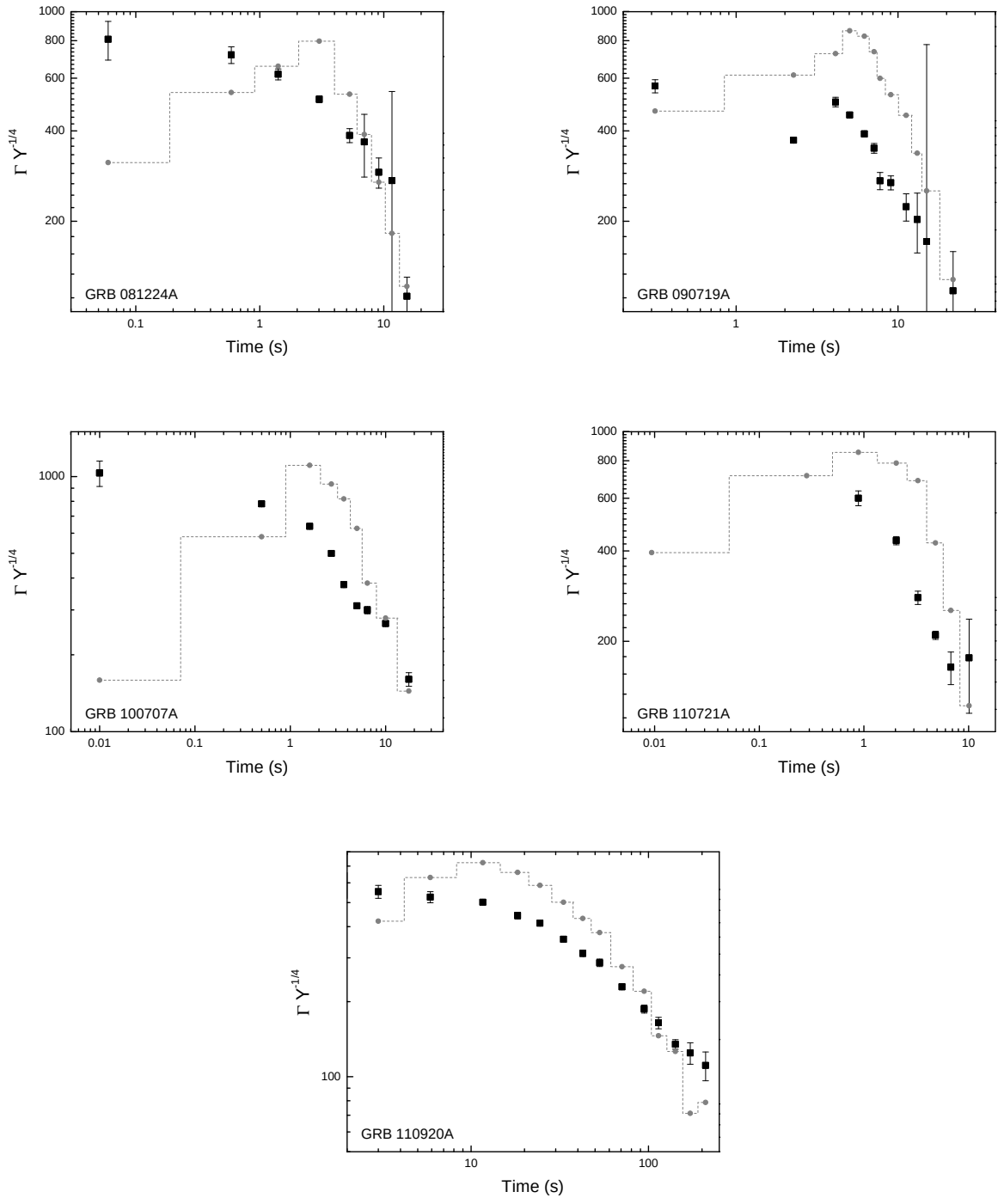

Figure 1. Evolution of Lorentz factor, $\Gamma\, Y^{-1/4}$, for five bursts, where $Y = L_0/L_{\rm obs,\gamma}$. The photon-flux light-curve (arbitrary units) is over-plotted in grey. Note that a blackbody component could not be detected during the first two time bins of GRB110721A.

measured blackbody flux and the total flux (blackbody + synchrotron), which generally is a good approximation for $F_{\rm BB}/F_{\rm kin}$, provided Y is close to unity. Since Y is unknown, these ratios are upper limits. The ratio initially lies around 40% (except for GRB110721A, see further discussion in §5.5) and typically decreases towards the end of the burst (see also Ryde & Pe'er (2009)). For GRB110920A, which has a significantly different pulse length, the ratio is shown in Figure 7 in Iyyani et al. (2015) and has a similar behaviour, with the ratio lying between 10 and 40%[2]. The blackbody components are thus very strong in four of the bursts and

[2] Iyyani et al. (2015) argues for a different physical interpretation

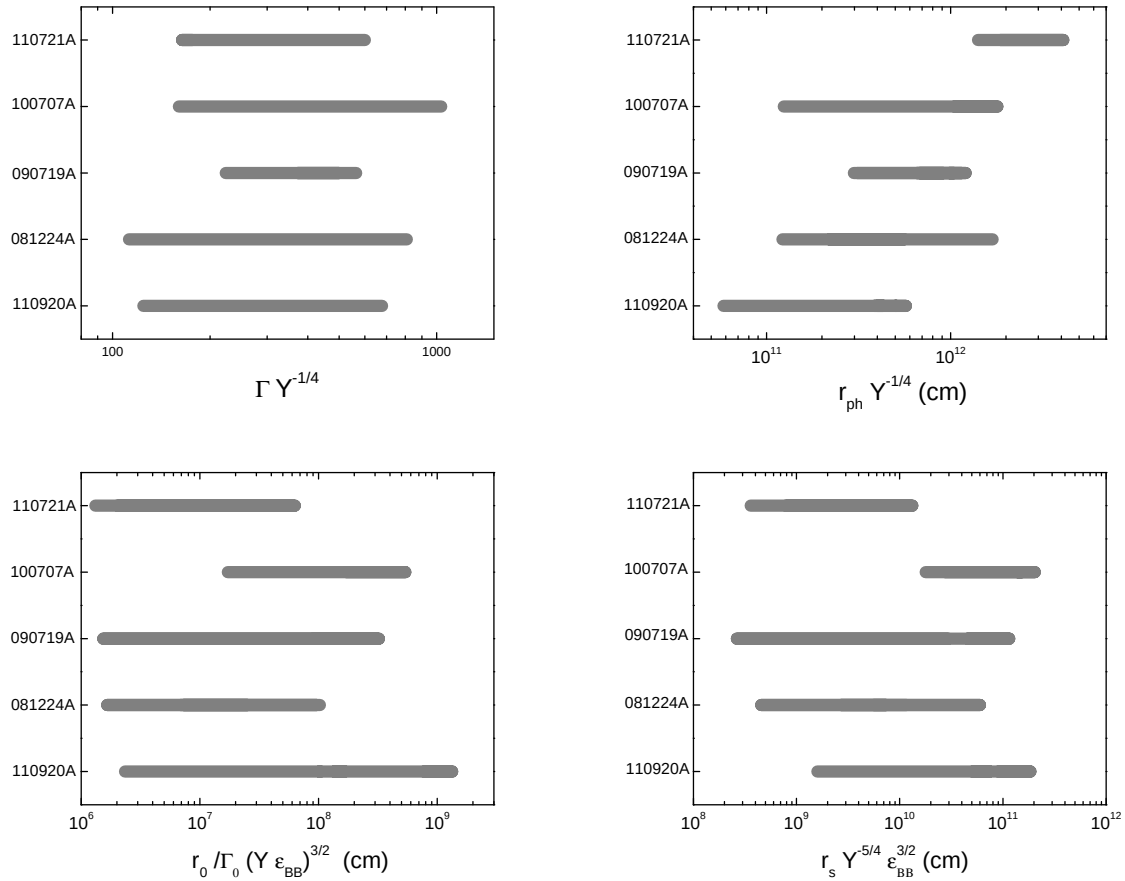

Figure 2. Ranges of the inferred outflow properties: $\Gamma Y^{-1/4}$ (upper left-hand panel), $r_{\rm ph}Y^{-1/4}$ (upper right-hand panel), $r_0/\Gamma_0(Y\epsilon_{\rm BB})^{3/2}$ (lower left-hand panel) and $r_{\rm s}Y^{5/4}$ (lower right-hand panel) for an assumed redshift, $z = 2$. Here Γ_0 is the Lorentz factor of the flow at r_0 and $\epsilon_{\rm BB}$ is the fraction of the burst energy that thermalises at the nozzle radius, r_0, of the jet (see Iyyani et al. (2013) for further details).

are comparable, to within a factor of two, to the archetypal baryonic photosphere burst GRB090902B which has an average ratio of 70% (Ryde et al. 2010; Pe'Er et al. 2012).

3 SYNCHROTRON COMPONENT

In this section, we study the variation observed in the properties of the non-thermal component, that is, the synchrotron component.

3.1 Observed Spectral Behaviour

Burgess et al. (2014) found that to produce acceptable spectral fits, a blackbody was required in addition to the synchrotron component in 5 of the bursts (see §1.1). In these cases, the C-stat improves by values > 10 in comparison to the synchrotron only fits, see Table 2 and 3 in Burgess et al. (2014). The presence of a blackbody in these bursts were found to be statistically significant, verified through simulations. The observed synchrotron peak, $E_{\rm sync}$, and the blackbody temperature, T, evolve as a broken power-law functions. In bursts GRB081224A, GRB090719A and GRB100707A the two breaks are consistent, while in GRB110721A and GRB110920A the breaks occur at different times.

On the other hand, there are three bursts (GRB081110A, GRB110407A and GRB090809A) that are consistent with a synchrotron component alone, where the improvement in C-stat for the addition of a blackbody component is less than 10. In these cases, the presence of a blackbody component could not be statistically validated by simulations. These bursts are also very bright and are not different from the other bursts in terms of their properties, such as peak energy and fluence. The observed synchrotron peak in these cases also evolve as a broken power-law.

Before discussing the constraints that these fits give, we review the basic points of synchrotron emission.

for this bursts, including thermal Comptonisation due to localised dissipation below the photosphere, see also §5.6.

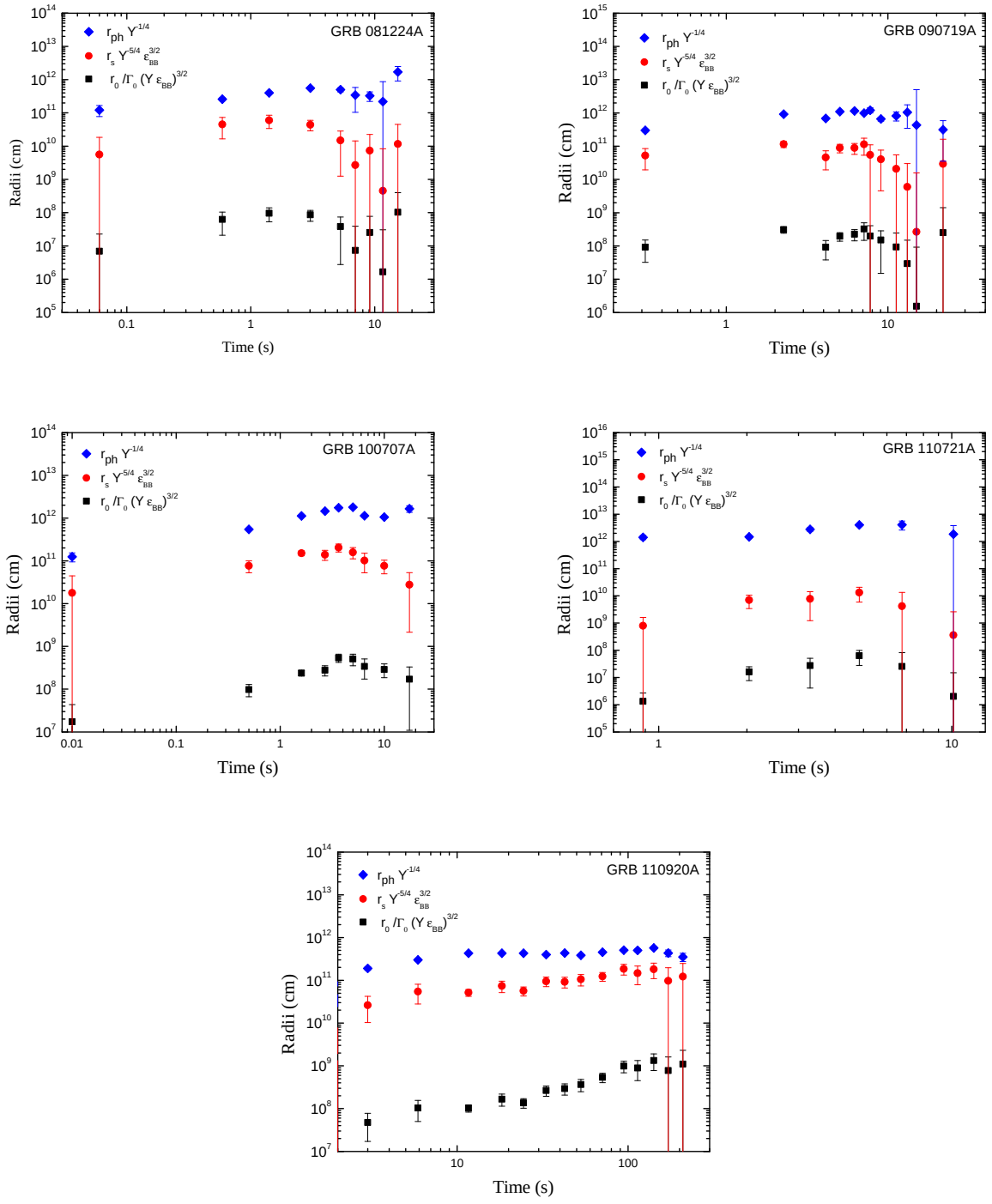

Figure 3. The evolution of the photospheric radius, $r_{\rm ph}Y^{-1/4}$ (blue diamonds), saturation radius, $r_{\rm s}Y^{5/4}\epsilon_{\rm BB}^{3/2}$ (red dots) and nozzle radius, $r_0/\Gamma_0(Y\epsilon_{\rm BB})^{3/2}$ (black squares). For details, see Figure 2.

3.2 Synchrotron emission

The dissipation of the kinetic energy of the outflow at a certain radius, r_d, causes the electrons to be accelerated to some characteristic Lorentz factor, $\gamma_{\rm el}$. The observed peak energy of synchrotron emission from these electrons is given by (see, e.g., Rybicki & Lightman (1986))

$$E_{\rm sync} = \frac{3}{2}\hbar\frac{qB}{m_e c}\gamma_{\rm el}^2\frac{\Gamma}{(1+z)} \quad (5)$$

where B is the magnetic field intensity in the comoving frame, m_e and q are the mass and charge of an electron, respectively, and $\hbar$ is the reduced Planck constant. The observed synchrotron flux is given by

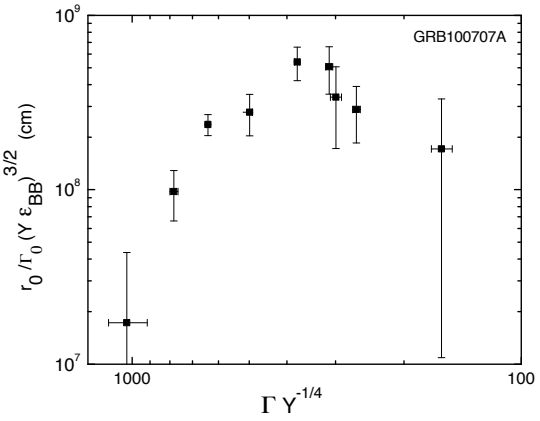

Figure 4. The correlation between r_0 and Γ for GRB100707A. The break in the correlation is mainly due to the break in the evolution of r_0 occurring at ~ 5 s (see Fig. 3).

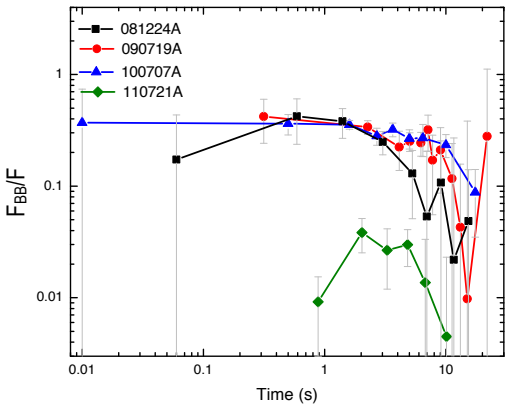

Figure 5. The ratio between the blackbody flux and the total flux (blackbody + synchrotron). A corresponding plot for GRB110920A is given in Figure 7 in Iyyani et al. (2015).

$$F_{\rm sync} = \frac{\sigma_T c \Gamma^2 \gamma_{\rm el}^2 B^2 N_e}{24\pi^2 d_L^2} \tag{6}$$

where N_e is the number of radiating electrons.

As the electrons emit radiation, they cool, and the radiative cooling time is given by (Sari et al. 1996)

$$t_{\rm cool} = \frac{6\pi m_e c}{\sigma_T B^2 \Gamma \gamma_{el}(1+\mathcal{Y})} \tag{7}$$

where $\mathcal{Y}$ is the Compton $\mathcal{Y}$-parameter and the factor $(1+\mathcal{Y})$ takes into account the cooling due to Compton scattering. The cooling time in equation (7) can be compared to the dynamical time,

$$t_{\rm dyn} \simeq \frac{R}{2\Gamma^2 c}. \tag{8}$$

Here, we assume that the conditions change on a timescale comparable to the dynamical timescale of the dissipation event. If $t_{\rm cool} < t_{\rm dyn}$ the electrons radiate efficiently and loose all their energy within the dynamical time (fast cooling) and if $t_{\rm cool} > t_{\rm dyn}$ the electrons do not efficiently radiate and thereby do not loose their energy during the dynamical time (slow cooling). The radiative efficiencies of the bursts in our sample are unknown. However, in recent years there is accumulating evidence, based on afterglow measurements, indicating that the efficiency of the prompt phase might be very high (Cenko et al. (2010); Racusin et al. (2011); Wygoda et al. (2015), however see Santana et al. (2014) and Wang et al. (2015)).

3.3 Constraints from the observations

From the spectral fits we have determined the peak of the synchrotron component, $E_{\rm sync}$, and for the five burst in which the thermal component is detected, we have determined the properties of the flow, for instance, the Lorentz factor, Γ and the photospheric radius, $r_{\rm ph}$ (see §2).

First, we find that the synchrotron energy peak [corrected for a redshift, $z = 2$, i.e $E_{\rm sync}\,(1+z)$] shows a correlation with Γ such that $E_{\rm sync}(1+z) \propto \Gamma^{2.17\pm0.12}$ (see

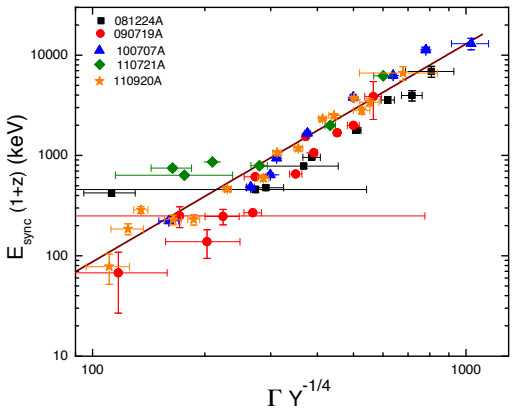

Figure 6. Peak energy of the synchrotron emission versus Lorentz factor correlation in the local frame (corrected for a redshift, $z = 2$). The correlation is given by $E_{\rm sync}(1+z) \propto \Gamma^{2.17\pm0.12}$.

Figure 6). However, according to equation (5), the peak energy $E_{\rm sync}(1+z) \propto \Gamma\gamma_{\rm el}^2 B$. Thus, the observed correlation suggests that $B\gamma_{\rm el}^2$ is approximately proportional to the evolution in Γ. This in turn suggests that both B as well as $\gamma_{\rm el}$ also evolve during the burst (Beniamini & Piran 2013; Uhm & Zhang 2014). In the analysis we take, in each time-bin, an average value of the magnetic field and $\gamma_{\rm el}$ (see further discussion in §5.1).

Second, assuming that the properties of the flow are the same at the photosphere and at the dissipation site, equation (5) then gives a constraint for the product $B\gamma_{\rm el}^2$ for every time bin in our observations:

$$B\gamma_{\rm el}^2 = \frac{E_{\rm sync}(1+z)4\pi m_e c}{\Gamma 3hq}. \tag{9}$$

These are shown by the black lines in Figure 7, where constraints obtained for three time bins are plotted: one before,

one at and one after the peak photon flux in order to capture the time evolution.

Furthermore, from equations (7) and (9), we can choose to express the cooling time as a function of $\gamma_{\rm el}$, which is plotted as blue lines in Figure 7 with the right hand (or blue) y-axis showing the cooling timescale. From equation (9), we find low values of B, for large values of $\gamma_{\rm el}$. Since cooling timescale, $t_{\rm cool}$ is very sensitive to the changes in B when these values are substituted in equation (7), result in longer cooling time even for large values of $\gamma_{\rm el}$. On the blue lines we mark with pink triangles $t_{\rm pulse}$ and the dynamical time (eq. 8) for $r_{\rm ph}$. In addition we plot the dynamical time for 10^{14}cm, representing a time between these extremes.

The red section of the lines show the values of B and $\gamma_{\rm el}$ that result in $t_{\rm cool} < t_{\rm dyn}(r_{\rm ph})$ for all allowed values of $r_d > r_{\rm ph}$. In other words, the electrons are always in the fast cooling regime. An upper limit of the dynamical time is given by the width of the pulse of the burst, $t_{\rm pulse}$ which corresponds to an upper limit of the allowed dissipation radius, $r_{d,\rm max} = 2\Gamma^2 c t_{\rm pulse}$. Thus, for values of B and $\gamma_{\rm el}$ depicted by the orange lines will always result in $t_{\rm cool} > t_{\rm pulse}$ (slow cooling) for the allowed values of r_d. The values of B and $\gamma_{\rm el}$ resulting in $t_{\rm dyn}(r_{\rm ph}) < t_{\rm cool} < t_{\rm pulse}$ (shown in black) can result in synchrotron emission from electrons either cooling fast or slow depending on where the dissipation occurs and what is the corresponding dynamical time.

The maximal spectral flux at the peak frequency is given by

$$\frac{F_{\rm sync}}{E_{\rm sync}} = \frac{\sigma_T \Gamma m_e c^2 B(1+z)\, N_e}{36\pi q d_L^2} \tag{10}$$

where $N_e = (8\pi\Gamma^2 r_d c t_{\rm dyn}\tau_e)/\sigma_T$ (Beniamini & Piran 2013). Thus, substituting for N_e in equation (10), the opacity of the electrons radiating synchrotron emission is given by

$$\tau_e = \frac{F_{\rm sync}}{E_{\rm sync}} \frac{9 q d_L^2\, \tau_{\rm tot}}{2\Gamma^3 m_e c^3 B\, r_{\rm ph} t_{\rm dyn}\, (1+z)} \tag{11}$$

where $\tau_{\rm tot} = r_{\rm ph}/r_d$ is the opacity due to the electrons associated to the number of baryons in the outflow at r_d. τ_e cannot be larger than $\tau_{\rm tot}$, unless electron - positron pairs are created via dissipation, and $t_{\rm dyn}$ at the maximum can only be the observed width of the pulse, $t_{\rm pulse}$. This gives a lower limit on B being between 10^{-3} and 10^{-4} G and thereby an upper limit on $\gamma_{\rm el}$ lying between $\sim$ few $\times\, 10^6$ and 10^8 (marked in green squares in Figure 7).

Since the best spectral fit is for synchrotron emission from uncooled electron distribution, the general requirements are $B < 1000$ G and $\gamma_{\rm el} > 10^4$ for all bursts in the sample. In particular, to be fully in the slow cooling regime, $\gamma_{\rm el}$ should be larger than between 10^5 and 10^6.

4 DECREASING Γ AND THE INTERNAL SHOCK MODEL

A common behaviour of the time-dependent analysis carried out here is that the Lorentz factor decrease in time (§2.1). This is a consequence of the characteristic temporal evolution of the temperature and thermal flux (Ryde 2004, 2005; Pe'er et al. 2007; Ryde & Pe'er 2009). Similar results were found in among others Ryde et al. (2010); Iyyani et al. (2013); Ghirlanda et al. (2013); Preece et al. (2014). Such a behaviour can be ascribed to varying central engine properties (see also Iyyani et al. (2013)). If this interpretation is correct, this behaviour excludes the possibility that the synchrotron emission component is from internal shocks since for these to occur later emitted shells of the jet have to catch up the preceding shells in order to form shocks. Therefore, in our interpretation the origin of synchrotron emission is from a forward shock. This is consistent with that all the bursts in sample are single pulses (Burgess et al. 2016, in prep.).

In the next sections, we discuss alternative assumptions that can be made in the derivation of the jet properties. In the estimations above we have assumed that the radiative efficiency and the magnetisation are constant over the burst. Moreover, we have assumed the flow to be baryon-dominated and have neglected high-latitude effects. Below, we investigate and discuss what happens if we relax these assumption.

4.1 Radiative efficiency: Y parameter

The radiative efficiency of the burst is given by Y^{-1} (eq. 3). In the estimations of Γ above, there is a dependence on the efficiency, $\Gamma \propto Y^{1/4}$ (eq. 2). Therefore, the determined evolution in $\Gamma(t)$ could, fully or in part, be attributed to corresponding variations in $Y(t)$. Estimations of Y can be made from afterglow measurements (Racusin et al. 2011; Wygoda et al. 2015). Unfortunately, for none of the bursts in the sample, afterglows have been observed.

We therefore study the limiting case where we assume that Γ remains a constant throughout the burst and determine what requirements then are set on Y. Since Y has to be greater than unity, the assumed constant value of Γ has to be larger or equal to the highest value of the currently estimated Γ . We now choose a value of constant Γ, equal to the highest value currently estimated. We then find the corresponding estimated value of Y to increase with time from nearly 1 to 1000.

This evolution of $Y(t)$, will affect the value of r_0 as well. We find that in all bursts then r_0 decreases from nearly 10^8 to 10^3 cm. As an example, the case of GRB100707A is shown in Figure 8. These values should be compared to the Schwarzschild radius of the central black hole, which is of the order of $10^{6.5}$ cm (for black hole of masses $5 - 10\, M_\odot$ Paczyński (1998)). Since the inferred values are smaller than the Schwarzschild radii, such an evolution of $Y(t)$ has to be rejected. Variations in the radiative efficiency can thus not account for the observed decrease in Γ. In addition to this, recently Wygoda et al. (2015) found that there is relative small scatter in the estimates of the radiative efficiency of bursts and find an average value of $Y \sim 2$. This suggests that large variations in Y within individual bursts are unlikely as well.

4.2 Magnetisation parameter, σ_0

The analysis above assumes that the magnetic field is subdominant. However, we have no way of directly measuring the magnetic field. It was shown by Zhang & Pe'er (2009) that if the magnetic field is dominant then the photospheric component is suppressed, which thus could explain the 4

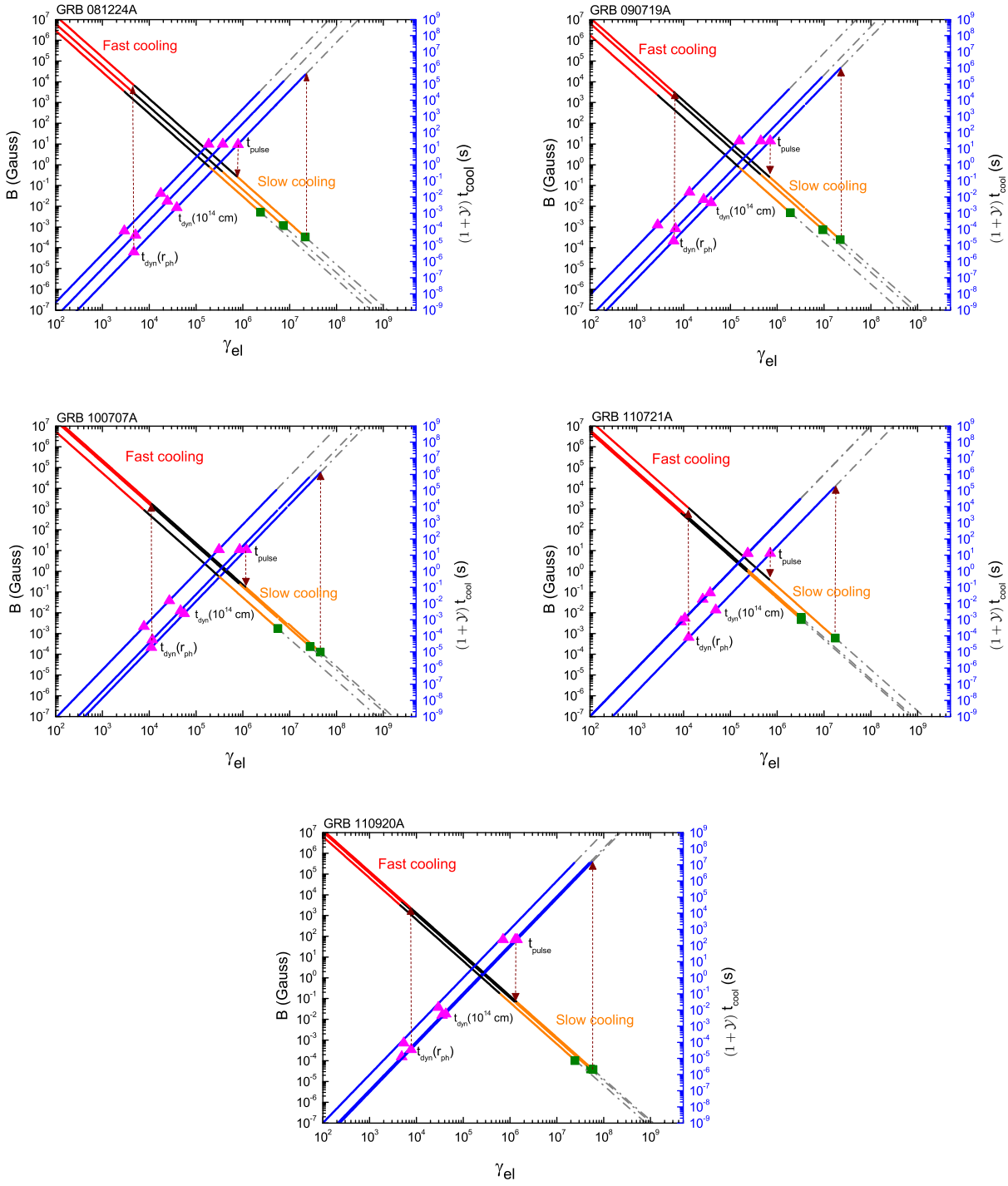

Figure 7. Allowed relations between B and $\gamma_{\rm el}$. The black lines show the constraints obtained for $B\gamma_{\rm el}^2$ from the equation (9) for three time bins: one before, one at and one after the peak of the light curve. The blue lines show the dependence of $t_{\rm cool}$ on $\gamma_{\rm el}$. The dynamical time for different characteristic radii ($r_{\rm ph}$, 10^{14}cm) and $t_{\rm pulse}$ are shown with pink triangles. The red section of the lines shows the values of B and $\gamma_{\rm el}$ that result in $t_{\rm cool} < t_{\rm dyn}(r_{\rm d})$ for all allowed values of $r_d > r_{\rm ph}$ i.e. the electrons always undergo fast cooling. The orange section of the lines shows the values of B and $\gamma_{\rm el}$ that will always result in $t_{\rm cool} > t_{\rm pulse}$, i.e, electrons always undergo slow cooling. The black part of the lines represents the condition where the cooling of the electrons can be either fast or slow depending at which radius the dissipation occurs. $\tau_e \leqslant \tau_{\rm tot}$ gives a lower limit on B and thereby a corresponding upper limit on the $\gamma_{\rm el}$, which is marked in green squares. The dash dot lines shown in grey on both the curves represent the forbidden parameter space of B, $\gamma_{\rm el}$ and $t_{\rm cool}$.

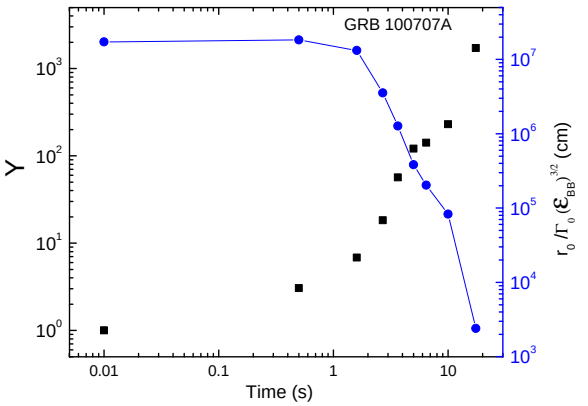

Figure 8. In order to keep the Lorentz factor a constant throughout the burst requires Y (black/ squares) to increase with time. This in turn implies that r_0 (blue/circles with line) has to decrease and reach unreasonably low values.

bursts with no or only a weak thermal component. On the other hand, as argued above, the presence of a strong thermal component with a flux $\sim 40\%$ of the observed total flux (see Figure 5) and at an energy well below 1 MeV, suggest that the outflow in these bursts are baryonic dominated. Still, for these bursts the outflow may be moderately magnetised. To investigate the effect of such a magnetisation on the derived parameters, we consider the hybrid model outlined in Gao & Zhang (2015) (see also Iyyani et al. (2013)), with a dominant baryonic component such that the outflow is predominantly accelerated by the thermal pressure. Moreover, for such a baryonically dominated outflow, there is a large paramerter space region in which the photosphere radius is above the coasting radius. In the following, we assume that this is the case, which corresponds to region III discussed in Gao & Zhang (2015).

In such a case, the total burst luminosity,

$$L_0 = L_h + L_c \tag{12}$$

where L_h is the hot component (fireball, characterised by $\eta \equiv L_h/\dot{M}c^2$) and L_c is the cold component (Poynting flux, characterised by σ_0) of the burst. The magnetisation parameter, σ_0 is defined as

$$\sigma_0 = \frac{L_c}{L_h} \tag{13}$$

The conditions $\sigma_0 \ll 1$ and $\eta \gg 1$ result in a pure fireball while $\sigma_0 \gg 1$ results in a highly magnetised outflow.

In this scenario, considering that there is no magnetic dissipation taking place below the photosphere, the outflow parameters are obtained as follows:

The Lorentz factor at the photosphere, $\Gamma_{\rm ph}$ is given by

$$\Gamma_{\rm ph} = \eta(1+\sigma_0), \tag{14}$$

see equation (12) in Gao & Zhang (2015). The photospheric radius, $r_{\rm ph}$, is given by

$$r_{\rm ph} = \frac{L_0\sigma_T}{8\pi m_p c^3 \Gamma_{\rm ph}^2 \eta(1+\sigma_0)}, \tag{15}$$

see equation (18) in Gao & Zhang (2015). Substituting equation (15) in equation (1) for $\mathcal{R}$ (see Pe'er et al. (2007)) gives the estimate of η of the burst,

$$\eta = \left[\frac{L_0\sigma_T\phi(1+z)^2}{8\pi m_p c^3 d_L (1+\sigma_0)^4 \mathcal{R}}\right]^{1/4} \tag{16}$$

for a given value of σ_0 and ϕ is a factor of order of unity. Once knowing η and substituting in equation (14) gives the estimate of $\Gamma_{\rm ph}$ and thereby $r_{\rm ph}$. It is worth noting that in this assumed scenario, the estimates of $\Gamma_{\rm ph}$ and $r_{\rm ph}$ have no dependence on the magnetisation parameter, σ_0 after the substitution for η, and the expressions obtained are equivalent to the ones obtained in Pe'er et al. (2007). The difference to be noted is that in this scenario $\Gamma_{\rm ph} \neq \eta$ which was otherwise the case in Pe'er et al. (2007).

The observed blackbody temperature, T, at the photosphere (see equation 22 in Gao & Zhang (2015)) is given by

$$T = \frac{\zeta\,\Gamma_{\rm ph}}{(1+z)} T_0 \left(\frac{r_{\rm ra}}{r_0}\right)^{-1} \left(\frac{r_s}{r_{\rm ra}}\right)^{-(2+\delta)/3} \left(\frac{r_{\rm ph}}{r_s}\right)^{-2/3} \tag{17}$$

where ζ is a factor of order of unity. The acceleration is initially mediated by the photons, at $r < r_{\rm ra}$, and at larger radii the acceleration is dominated by the reconnection by the magnetic field, resulting in $\Gamma \propto r^{\delta}$ ($\delta = 1/3$) until the saturation radius r_s.

$$T_0 = \left(\frac{L_0}{4\pi r_0^2 c a (1+\sigma_0)}\right)^{1/4} \tag{18}$$

where a is the radiation constant and

$$r_s = r_{\rm ra}\left(\frac{\Gamma_c}{\Gamma_{\rm ra}}\right)^{1/\delta} \tag{19}$$

where $\Gamma_{\rm ra} = r_{\rm ra}/r_0$. One can use the expression in equation (17), and after some algebra, solve for the nozzle radius of the jet, r_0:

$$r_0 = \psi\,\frac{\mathcal{R}\,d_L}{(1+z)^2}\left(\frac{F_{\rm BB}}{F}\right)^{3/2}\left(\frac{1+\sigma_0}{Y}\right)^{3/2} \tag{20}$$

where ψ is a factor of order of unity.

In summary, if we assume a value for σ_0, we can estimate the outflow parameters r_0, η and thereby $\Gamma_{\rm ph}$. However, in this scenario we cannot estimate r_s as $r_{\rm ra}$ is unknown.

A general assumption that is made in the literature is that r_0 is the size of the central engine and remains constant through out the burst duration. If we assume r_0 to be a constant, we explore the variation that is possible in the unknown quantity $(1+\sigma_0)/\epsilon_{\rm BB}Y$ which we parameterise as χ. Figure 9a, for the case of GRB100707A, shows that when $r_0 = 2\times10^7$ cm throughout the burst, the χ varies between values 1 and 0.1. This clearly rules out any possibility of having σ_0 much larger than 1 (if $Y \sim 1$) which means the burst is weakly magnetised. Figure 9b shows that when we assume $r_0 = 10^9$ cm, we find χ to vary between 15 and 1.5. This implies that the $\sigma_0 > 1$; however since it is not $\sigma_0 \gg 1$, in such a case the burst is only moderately magnetised. This is consistent with the fact that we observe a strong blackbody component in the spectrum.

In conclusion, for the bursts with strong thermal components, the decreasing Lorentz factor can neither be due to a varying radiative efficiency nor a varying magnetisation of the jet (assuming the photosphere radius is above

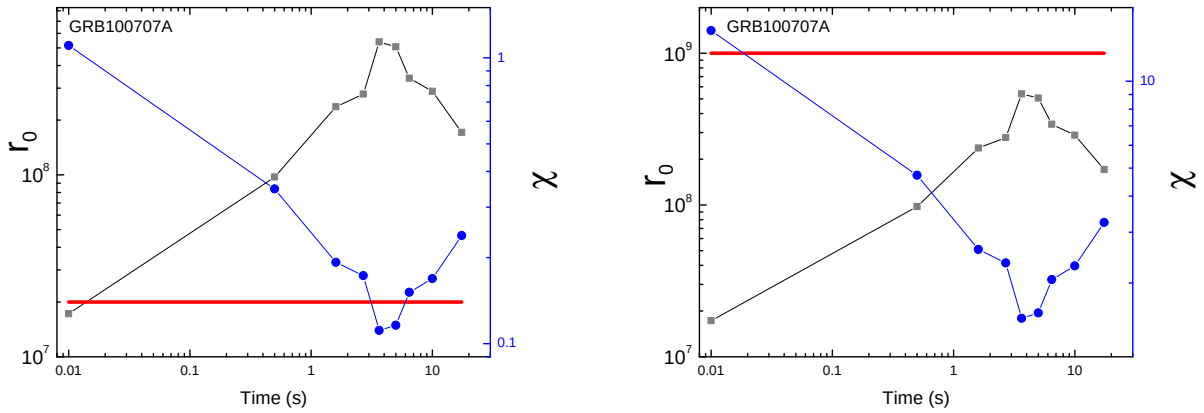

Figure 9. If r_0 is assumed to be a constant throughout the burst duration at $r_0 \sim 2 \times 10^7$cm, marked in red solid line (left hand panel) or $r_0 \sim 10^9$cm, marked in red solid line (right hand panel), we find $\chi \equiv (1+\sigma_0)/\epsilon_{\rm BB} Y$, which gives a measure of the magnetisation of the outflow, to evolve as shown (blue circles with line). The otherwise deduced evolution of r_0 is shown in shade (grey squares with line).

the coasting radius). For the other bursts we have very poor constraints on the magnetic field. For the three bursts where we did not have any clear detection of thermal component we did not carry out any analysis, while for GRB110721A we perform a similar analysis to the others. This can be justified by the fact that a subdominant thermal component does not necessary mean that the magnetisation is high. We point out that an alternative analysis for GRB110721A has been carried out by Gao & Zhang (2015), see (§5.5).

5 DISCUSSION

5.1 Electron acceleration and magnetic field strength

Within the interpretation of the spectrum presented here a large part of the spectrum is due to synchrotron emission. Since the electron distribution appears to be in the slow cooling regime, this sets strong limitations on the typical energy of the radiating electrons, for instance the minimum electron Lorentz factor, $\gamma_{\rm el} \equiv \gamma_{\rm min}$ should be larger than 10^5 to 10^6 (see also Beniamini & Piran (2013)). Such values are much larger than the typically assumed values, up to $\gamma_{\rm min} \sim m_{\rm p}/m_{\rm e} = 1836$, expected in various internal shock scenarios (Bošnjak et al. 2009), but are more typical for what is expected for forward shocks, see §5.2.

One possibility is that only a small fraction of the electrons receive the dissipated energy and are accelerated forming a power law distribution with $\gamma_{\rm min} \gg m_{\rm p}/m_{\rm e}$ disconnected to the thermal distribution of electrons (Daigne & Mochkovitch 1998; Beniamini & Piran 2013). It is only the energetic electrons which radiate and the thermal electrons do not participate in the emission. However, simulations of collisionless shocks show that most of the electrons are accelerated and form a Maxwellian distribution with only a small contribution from a power law tail (Spitkovsky 2008).

It can also be imagined that the electrons are in the fast cooling regime, however their distribution is maintained through a balance between heating and cooling. Since the flow is baryonic (based on the observation of the BB component) the heating is mainly assumed to be due to shocks. Baryonic shocks, however, cannot maintain such a balance since the shocked particles will rapidly leave the shocked zone and cool undisturbed (Ghisellini & Celotti (1999), see also Kumar & McMahon (2008)). On the other hand, in a scenario suggested by Pilla & Loeb (1998); Medvedev & Loeb (1999), there can be an extended shock scenario where the shocked region is extended over a large volume due to Rayleigh -Taylor instability (see also Duffell & MacFadyen (2014b)). In such a case, the mean energy of electrons would be dictated by the balance between heating and cooling and this would result in values of $\gamma_{\rm min} < m_p/m_e$. This in turn from equation (9) requires that the magnetic field, $B > 10^4$G (see Figure 7).

Another way of relaxing the condition of slow cooling and still maintaining the observed electron distribution is a marginally fast cooling scenario (Daigne et al. 2011). Here the characteristic Lorentz factor of electrons, when the cooling time is equal to the dynamical time, $\gamma_c \leqslant \gamma_{\rm min}$, which is opposed to the requirement of $\gamma_c \ll \gamma_{\rm min}$ for the fast cooling regime. The spectral peak is formed at $\nu_{\rm c,eff}$ such that the photon index below $\nu_{\rm c,eff}$ is $-2/3$ (slow cooled) even when in the fast cooling regime. However, such a cooling tends to occur at large radii where the magnetic field, B is low and the outflow has a large Lorentz factor. In our analysis, we find B to be large for the case where fast cooling condition is satisfied (i.e $t_{\rm cool} < t_{\rm dyn}$) and thus, suggests that the cooling may not be marginally fast cooling. This also requires fine tuning in order to get $\gamma_c \leqslant \gamma_{\rm min}$.

In the spectral fits discussed in this paper the synchrotron component is associated with a certain value of the magnetic field strength. The underlying assumption is that the magnetic field is constant in the emission region and does neither take into account inhomogeneities of the field strength nor the possibility of an evolving magnetic field or of an evolving injection rate of electrons. A possibility to address the large values of $\gamma_{\rm min}$ is therefore a scenario where the plasma is inhomogenous such that the magnetic field

strength varies in different regions of the flow and the electrons emit radiation only when in the regions of strong magnetic field (Pe'er & Zhang 2006; Beniamini & Piran 2014). In such a scenario, the electrons can escape the emitting regions before they have the time to cool significantly and thus remain uncooled. Since only a small fraction of the energy stored in the electrons is radiated away, the energy budget is severely strained.

Uhm & Zhang (2014) suggested a model in which the emission region streams outwards in an expanding jet and therefore the magnetic field strength in the emission region decreases with radius [$B(r) \propto r^{-b}$], with $b \sim 1 - 1.5$. The great advantage of such a model, compared to traditional synchrotron models, is that it has a physical prescription to explain the observed curvature and shape of the spectra in terms of varying magnetic field. Zhang et al. (2015) uses such a model to fit the spectra of GRB130606B and find that it can fit the data well, provided a large value of $\gamma_{min} \sim 10^5$. In addition, they find that, in order to explain the spectra with the Band function $\alpha \sim -0.8$, a rapid increase in the electron injection rate is needed; $Q_\gamma \propto t^q$, with values up to $q \sim 4$. This means that even though the electrons are in the fast cooling regime initially (large B field, low injection rate) the dominant contribution to the observed spectra is from emission when the electrons are in a low magnetic field environment, with a correspondingly longer cooling time. The narrowness of the spectrum forces the synchrotron fits, from this scenario, to largely resemble the slow-cooled synchrotron spectrum of Burgess et al. (2014).

5.2 Forward Shock Origin

In a baryonic outflow the kinetic energy is typically assumed to be extracted by internal shocks. However, emission from external, forward shocks could be important during the prompt phase for smooth pulsed GRB (Panaitescu & Mészáros 1998; Burgess et al. 2015). Similary, Duffell & MacFadyen (2014a) finds from simulating the jet ($\Gamma \geqslant 100$) passing though the progenitor star, that a baryon loaded shell lies in front of the jet head at breakout moving with $\Gamma_{\rm shell} \sim 10$. As they collide, highly efficient internal shocks are produced. The internal shocks are then produced until a radius $\sim 10^{16}$ cm. In both cases, the shocks produced results in synchrotron emission with $\gamma_{\rm min} \sim (m_{\rm p}/m_{\rm e})\,\Gamma$, which now is more consistent with the inferred values from the observations.

In the external shock scenario the evolution observed for the non-thermal component is independent of that of the thermal component. The inferred initial Lorentz factor (Γ_0) from the evolution of the synchrotron component, would not be larger than the largest Γ value inferred from the thermal component at the photosphere. The estimation of the outflow parameters at the photosphere at later times during the decay phase of the pulse is not possible, as the total flux corresponding to each time bin is not known explicitly.

The observed variability of the thermal component with time tells us how the central engine varies with time. Following the arguments in §2.2, we find that during the rising phase of the pulse if Γ remains nearly steady, the baryon load of the outflow is increasing with time. As a result we can expect high inertia shells to be ejected by the central engine in the beginning of the burst. This high inertia shells then crash into the external medium and results in the shocks which then produce the observed synchrotron emission. During the decay phase, as luminosity of the burst is decreasing, the shells ejected by the central engine have lower Γ and thereby may not catch up with the external, forward shocks that had been produced. Instead, they may be decelerated by the reverse shocks that have been produced. A more detailed discussion in this scenario is given in Burgess et al. (2015).

5.3 Evolution of r_0

Shear turbulence and oblique shocks within the stellar core can result in r_0 attaining values much larger than the expected size of the central engine (e.g., Thompson et al. (2007); Iyyani et al. (2013); Pe'er et al. (2015)). Indeed, several hydrodynamical simulations have shown that there are significant collimation shocks produced within the outflow as the jet traverses through and emerges out of the stellar cocoon (Mizuta & Ioka 2013a; López-Cámara et al. 2013; Zhang et al. 2003; Lazzati et al. 2015). It is also interesting to note that the variability time scale that are found in GRB light curves are consistent with the large r_0 values derived above. For instance, Golkhou & Butler (2014) find the typical minimum variability time scales, Δt, to be of the order of a fraction of a second, with a shortest time scale of 10 ms. Such a time scale corresponds to a size of the central engine between $r < c\Delta t_{\rm min} \sim 3 \times 10^8$ cm and 2×10^{10} cm.

Iyyani et al. (2013) suggested that a larger outflow velocity (or Γ) would prevent the formation of such shocks and thus result in smaller values of r_0. Most of the bursts in the sample have r_0 that evolve like a pulse with time. Thus, it may be speculated that during the period where r_0 increases and shows a negative correlation with Γ, the position of r_0 may be determined by such shocks when the jet is propagating through the progenitor envelope (Beloborodov 2013; Lazzati et al. 2009; Mizuta & Ioka 2013b). Beyond the core radius of the star, the oblique shocks due to the confinement of the jet by the cocoon of the progenitor becomes weak and less efficient. As a result, r_0 does not increase any further, instead decreases or remains nearly steady. However, there have been no direct simulation study done to evaluate how r_0 evolves during a GRB mainly due to the limitations of numerical simulations on these scales.

It has been suggested by Ghisellini et al. (2007) that shocks are produced in the outflow when it encounters the cocoon material surrounding the progenitor, which is in the way of the jet. As a result, the fireball is reborn at a larger radius, i.e, the surface of the progenitor. If we associate r_0 to the surface of the progenitor, in such a case it may be speculated that with time as the stellar material surrounding the black hole gets accreted, we would expect r_0 to decrease. In accordance to this, we find that after r_0 reaches its peak value, it then decreases and thereby shows a positive correlation with Γ.

Yet another alternative explanation to the observed temporal behaviour of r_0 is propagation effects of the jet inside the collapsing star. The jet expansion is actually not expected to be free, but is affected by various effects such as multiple recollimation shocks, mass entrainment, or a non-conical structure of the flow. In such a case, the interpre-

tation of the value of r_0 as well as its evolution will have another meaning.

5.4 High latitude effects on the evolution of temperature and flux

It was proposed by Pe'er (2008); Pe'er & Ryde (2011) that the origin of the late time decay of the thermal flux and the temperature (Ryde 2004, 2005; Ryde & Pe'er 2009), may be associated with off-axis emission, which is seen at a delay with respect to the emission from the jet axis. Furthermore, the late time photons are observed at lower energies due to the lower Doppler boost and larger photospheric radius (which is angle-dependent). However, as was pointed out by Deng & Zhang (2014), for spherical outflows with parameters characterising GRBs, the characteristic time-scale for the decay is faster than observed here. This issue may be resolved if one introduces angular structure of energy and Lorentz factor of the jet (Beloborodov 2010, Lundman et al. (2013)), although detailed calculations and hence firm conclusions are still lacking.

5.5 Poynting-flux dominated outflows

Even though a strong photospheric emission component disfavours Poynting-flux dominated flows, since the energy of such a component would be suppressed by a factor of $(1+\sigma)^{-1}$ (Zhang & Pe'er 2009), one cannot rule out such a possibility. If, e.g., the radiative efficiency is low (i.e large Y parameter) the actual ratio of the thermal to kinetic energy might be smaller than estimated from the data. Furthermore, in Poynting-flux dominated flows many of the problems faced by synchrotron emission in baryonic flows, and discussed in §5.1, can naturally be overcome. As pointed out by Zhang & Yan (2011) a balance between heating and cooling is expected to be established by second-order stochastic acceleration in the turbulent region of the ICMART scenario (Internal-Collision-Induced Magnetic Reconnection and Turbulence). Moreover, the number of baryons associated electrons is smaller by a factor of $\sim (1+\sigma)^{-1}$, and therefore every electron naturally attains a higher Lorentz factor.

In order to estimate the flow parameters and their evolution, as done above for the baryonic dominated case, a more generalised formalism is needed. This is because, if the Poynting flux dominates the energy of the flow, the dynamics will change. For instance, the large fraction of the acceleration phase will have a more gradual acceleration compared to the initial, thermal acceleration. Moreover, the photosphere will most likely occur while the flow is still accelerating. The general formalism introduced by Gao & Zhang (2015) covers all these different possible cases. Additional assumptions have to be made, though, in order to estimate the flow properties. First, further unknowns are introduced (e.g., the magnetisation of the flow σ). Second, since the acceleration of the flow is assumed to occur in phases with different radial dependencies and since these dependencies are not yet fully understood (see, e.g., Bromberg & Tchekhovskoy (2015)) an assumed prescription is needed to be made.

Gao & Zhang (2015) applied this formalism to GRB110721A, whose thermal flux component is only at a few per cent level (see Fig. 5), which is consistent with a Poynting-flux dominated interpretation. They make the assumption of a constant value for r_0 (choosing several different values), which allows them to use the observables to derive the flow parameters. With the choice of $r_0 \sim 10^8$ cm, they find that the magnetisation has to vary in strength by nearly 2 orders of magnitude, with the flow changing from being highly magnetised at the photosphere, $(1+\sigma_{ph}) \sim 100$, to being depleted of the magnetic field (kinetic energy dominates the flow), $(1+\sigma_{ph}) \sim 1$, at around 2.5 s. At this point, the initial magnetisation is also found to be weak $(1+\sigma_0) \sim 1.5$, which indicates that the acceleration is mainly thermal and that the behaviour approaches that of a baryonic flow. This is consistent with the fact that r_0 in Fig. 3 (assuming a baryonic flow) approaches this assumed value of $\sim 10^8$ cm.

There are thus two interpretations for the spectral evolution in GRB110721A, a baryonic-dominated flow (this paper and Iyyani et al. (2013)) and a Poynting-flux dominated flow (Gao & Zhang 2015). The former interpretation yields a varying r_0, which is interpreted as being caused by recollimation shocks as the jet traverses within the star, see §5.3. In the latter interpretation, the flow is Poynting flux dominated and the spectral evolution is explained by a varying magnetisation, while keeping r_0 fixed. The theory of magnetised outflow, however, is not fully developed. For example, it is not obvious as to which value of r_0 should be chosen.

The fraction of bursts in which a strong and/or statistically significant thermal component exists is debatable. In the strongest, single pulsed bursts studied above, 4 out of 8 have such a strong thermal component, such that the magnetic content of the jet cannot be dominant. On the other hand, the four bursts, in which there are no strong detections of blackbodies, are consistent with Poynting flux-dominated outflows, yeilding a synchrotron spectrum. We point out that in similar cases to these bursts, the width of the spectrum is essential to estimate, since there is a hard limit to how narrow a synchrotron spectrum can be, see §5.4 and Axelsson & Borgonovo (2015); Yu et al. (2015).

5.6 Subphotospheric dissipation

This study has interpreted the prompt GRB spectrum in a two-emission-zone model where the blackbody component is from the photosphere and the synchrotron component is from the optically-thin region (see also Ryde (2005); Guiriec et al. (2013); Iyyani et al. (2013); Burgess et al. (2014); Preece et al. (2014)). Such an interpretation describes a totally different physical scenario compared to the one invoked by a fitting model in which the full spectrum is due to subphotospheric dissipation (Ryde et al. (2010); Iyyani et al. (2015); Ahlgren et al. (2015)). In the latter scenario, all emission stems from the photosphere which no longer forms a blackbody. Due to dissipation of the kinetic energy of the flow in a region below the photosphere the emission spectrum can be significantly broader and have complex shapes (Pe'er & Waxman 2005; Beloborodov 2010).

In many cases, both the models are consistent with the data. This ambiguity in the interpretation of the data is illustrated here for the case of bursts GRB081110A and GRB110920A. GRB081110A is one of the bursts in the sample that is consistent with the synchrotron emission alone,

while GRB110920A shows evidence for an additional blackbody component. In Figure 10, we show the spectral fit to the time bin at its peak flux, when modelled using a Band function alone (orange solid line) and a synchrotron function alone (green solid line), where the shaded region shows the uncertainty in the shape of the spectrum related to each model respectively. It is interesting to note that due to the large flexibility of the Band function, the Band function fit to the spectrum results in a spectral shape that is narrower at full width half maximum (FWHM) of the νF_ν peak, than the synchrotron function. Such a spectrum is more easily interpreted in a subphotospheric dissipation scenario, which is not limited by the fundamentally required width for synchrotron emission. However, we find that statistically both the models are consistent with the data. In such cases, it becomes important to explore the implications of each model within its related physical scenario which need to be validated if the resultant physical conditions are feasible or not.

Further, elaborating this fact of complication involved in the interpretation of various models fitted to the spectrum, in Figure 11, we show the comparison of the spectral fits to the spectrum of GRB110920A with the models: Comptonisation + power law (pink solid line), which represents the photospheric emission including localised subphotospheric dissipation at moderate optical depths (Iyyani et al. 2015), and blackbody + synchrotron emission (green solid line), which represents the two-emission-zone model. Figure 11 clearly shows that these two models result in two different spectral shapes, however, both the spectral shapes are consistent with the data. We note that, in this particular case, we find the narrowness of the spectrum at the νF_ν peak is highly constraining, since in blackbody + synchrotron fit, the spectral width at FWHM is given by the blackbody component, which thus confirms the fact that the νF_ν peak of the spectrum is actually very narrow. This, again points out the fact that a spectrum which has a narrow νF_ν peak, still may be consistent with a synchrotron emission, however, only with a dominant blackbody emission which is observed in this case. We also note that from a statistical (C-stat) point of view, we find Comptonisation + power law to be a better model. However, since both the models are differently motivated, the statistical comparison is largely indecisive. The acquired observational behaviour needed to be physically validated, in order to clearly ascertain which is the best spectral model. This in turn requires the existing GRB theories to have clear predictions in regard to the temporal behaviour of the outflow in their respective physical picture.

Fitting physical models is an important step forward in comparison to empirical model fitting which is the most common approach today. However, due to the ambiguity between models we have to resort to assessing the models from a theoretical perspective by considering the constraints that observations set. For instance, in the synchrotron fits above, the data strongly disfavours a typical fast cooling scenario. Slow cooling is permitted but sets strong constraints on the acceleration process needed such that only a small fraction of the electrons are accelerated to very high energies. Moreover, the emission would be greatly inefficient. This points towards reheating of the electrons causing a steady state electron distribution which produces a slow-cooling-like spectrum. The physical scenario needs to be addressed in order to assess the validity of the fit results.

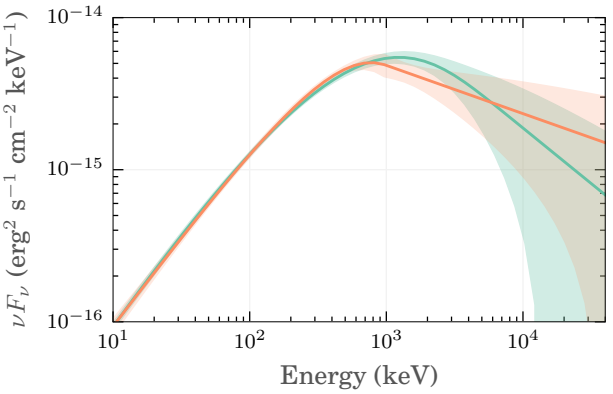

Figure 10. The spectral fits to the time-bin at the peak flux of GRB081110A: The Band function fit is shown by the orange solid line and the synchrotron fit is shown by the green solid line. The shaded regions depict the uncertainty in the spectral shapes of the respective model. The Band function results in a spectral shape that is narrower at the νF_ν peak as compared to the shape of the synchrotron function.

Another weakness of the two-zone scenario presented above is the use of a blackbody for the photospheric component. The observed emission from the photosphere is expected be a multicolour blackbody (Beloborodov 2010). Along with that, including the effects of a GRB jet observed at different viewing angles can give rise to a much broader spectrum, see Lundman et al. (2013). Moreover, there can also be dissipation of the kinetic energy of the flow below the photosphere. In such a case, the blackbody will be significantly broadened and the physical validity of the blackbody+synchrotron model will fall. However, there is a small but significant fraction of bursts that are indeed fitted with a single blackbody (Ryde 2004; Ghirlanda et al. 2013; Larsson et al. 2015) which suggests that the emission from the photosphere under certain circumstances can be a blackbody. Moreover, the blackbody component used in the fits does not need to reflect the true shape but rather capture a peaked spectrum appearing above the synchrotron emission.

6 CONCLUSIONS

We have investigated the fits to the GRB spectral data of a sample of 8 single pulsed GRBs, with models involving synchrotron emission. Two immediate requirements apply: (i) a photospheric component (blackbody) is strong in four out of eight bursts and statistically highly significant, while subdominant, in another one and (ii) the energy distribution of the radiating electrons have to be in the slow cooling regime or be reheated. The need for a strong blackbody suggests that the flow is baryonic-dominated, at least in four of the cases. Furthermore, we find a robust trend that the Lorentz factor of the flow decreases with time during the burst which can neither be explained by a varying radiative efficiency nor a varying magnetisation of the jet making the reasonable assumption that the photosphere radius is above

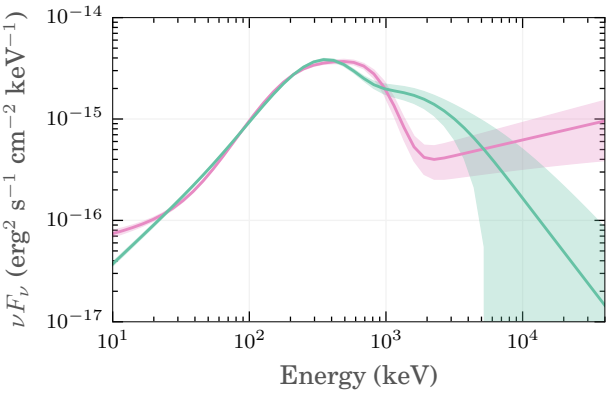

Figure 11. The spectral fits to the time-bin at the peak flux of GRB110920A: Comptonisation + power law model of Iyyani et al. (2015) is shown by the pink solid line and the blackbody+synchrotron model is shown by the green solid line. The spectral shapes resulting from the two models are clearly different. The shaded regions depict the uncertainty in the spectral shapes of the respective model.

the coasting radius). Such a behaviour is contradictory to what is expected from various internal shock scenarios. We also find a strong trend that the distance from the central engine to the flow nozzle can attain large values (typically $10^8 - 10^9$ cm) and increase with time. This gives a prediction to the properties of the jet at the very core of the progenitor star.

The non-cooled electron distribution, required from the fits, can be due to the cooling time being larger than the typical dynamical time (slow cooling). In such a case only a small fraction of the electrons should be accelerated to very large Lorentz factors or the energy dissipation should be due to forward shocks. The radiative efficiency would by necessity then be low in these cases. Alternatively, the electron distribution can be attained through a balance between heating and cooling. However, this is typically not expected in baryonic shocks, even though a scenario of extended shocks have been described, and therefore, needs further investigation to verify its plausibility. Finally, a scenario where the plasma is inhomogenous such that the magnetic field strength varies have been suggested. Further fits to data with such physical models are needed to assess their validity.

We point out that alternative physical models, for which the synchrotron component is not needed at all, are also consistent with the data. In particular, scenarios including subphotospheric dissipation afford to give physically plausible explanations of the data. However, such models need to explain the inferred radial distribution of dissipation, for instance, through numerical simulations. The fits cannot distinguish between these models decisively from a statistical point of view and the distinction must be made using arguments regarding their physical plausibility. Finally, we have also pointed out that in order to test the viability of synchrotron emission in the observed data, a Band function is not sufficient.

ACKNOWLEDGEMENTS

We thank the referee, Dr. Bing Zhang, for very thorough and useful comments on the manuscript. We acknowledge support from the Swedish National Space Board and Swedish Research Council (Vetenskapsrådet). SI is supported by the Erasmus Mundus Joint Doctorate Program by Grant Number 2011-1640 from the EACEA of the European Commission. DB is supported by a grant from Stiftelsen Olle Engkvist Byggmästare. AP acknowledges support by the European Union Seventh Framework Programme (FP7/2007-2013) under grant agreement no 618499.

REFERENCES

Ahlgren B., Larsson J., Nymark T., et al. 2015, MNRAS, 454, L31
Asano K., Terasawa T., 2009, ApJ, 705, 1714
Axelsson M., Baldini L., et al. 2012, ApJ, 757, L31
Axelsson M., Borgonovo L., 2015, MNRAS, 447, 3150
Bagoly Z., Mészáros A., et al. 2006, A&A, 453, 797
Baring M. G., Ellison D. C., Jones F. C., 1995, Advances in Space Research, 15, 397
Bégué D., Pe'er A., 2015, ApJ, 802, 134
Beloborodov A. M., 2010, MNRAS, 407, 1033
Beloborodov A. M., 2013, ApJ, 764, 157
Beniamini P., Piran T., 2013, ApJ, 769, 69
Beniamini P., Piran T., 2014, MNRAS, 445, 3892
Bošnjak Ž., Daigne F., Dubus G., 2009, A&A, 498, 677
Bromberg O., Tchekhovskoy A., 2015, ArXiv e-prints
Burgess J. M., Bégué D., et al. 2015, ArXiv e-prints
Burgess J. M., Preece R. D., Connaughton V., et al. 2014, ApJ, 784, 17
Burgess J. M., Ryde F., Yu H.-F., 2014, ArXiv e-prints, 1410.7647
Cenko S. B., Frail D. A., et al. 2010, ApJ, 711, 641
Daigne F., Bošnjak Ž., Dubus G., 2011, A&A, 526, A110
Daigne F., Mochkovitch R., 1998, MNRAS, 296, 275
Deng W., Zhang B., 2014, ApJ, 785, 112
Drenkhahn G., Spruit H. C., 2002, A&A, 391, 1141
Duffell P. C., MacFadyen A. I., 2014a, ArXiv e-prints, 1407.8250
Duffell P. C., MacFadyen A. I., 2014b, ApJL, 791, L1
Gao H., Zhang B., 2015, ApJ, 801, 103
Ghirlanda G., Ghisellini G., et al. 2013, MNRAS, 428, 1410
Ghisellini G., Celotti A., 1999, ApJL, 511, L93
Ghisellini G., Celotti A., Ghirlanda G., Firmani C., Nava L., 2007, MNRAS, 382, L72
Goldstein A., Preece R. D., Mallozzi R. S., Briggs M. S., Fishman G. J., Kouveliotou C., Paciesas W. S., Burgess J. M., 2013, ApJS, 208, 21
Golkhou V. Z., Butler N. R., 2014, ApJ, 787, 90
Guiriec S., Connaughton V., et al. 2011, ApJL, 727, L33
Guiriec S., Daigne F., Hascoët R., Vianello G., Ryde F., Mochkovitch R., Kouveliotou C., Xiong S., Bhat P. N., Foley S., Gruber D., Burgess J. M., McGlynn S., McEnery J., Gehrels N., 2013, ApJ, 770, 32
Hascoët R., Daigne F., Mochkovitch R., 2013, A&A, 551, A124
Iyyani S., Ryde F., Ahlgren B., Burgess J. M., Larsson J., Pe'er A., Lundman C., Axelsson M., McGlynn S., 2015, MNRAS, 450, 1651

Iyyani S., Ryde F., Axelsson M., Burgess J. M., et al. 2013, MNRAS, 433, 2739
Katz J. I., 1994, ApJL, 432, L107
Kumar P., McMahon E., 2008, MNRAS, 384, 33
Larsson J., Racusin J. L., Burgess J. M., 2015, ApJL, 800, L34
Lazzati D., Morsony B. J., Begelman M. C., 2009, ApJL, 700, L47
Lazzati D., Morsony B. J., López-Cámara D., 2015, ArXiv e-prints
Liang E. P., Jernigan T. E., Rodrigues R., 1983, ApJ, 271, 766
López-Cámara D., Morsony B. J., Begelman M. C., et al. 2013, ApJ, 767, 19
Lundman C., Pe'er A., Ryde F., 2013, MNRAS, 428, 2430
McGlynn S., Fermi GBM Collaboration et al. 2012, in -Ray Bursts 2012 Conference (GRB 2012) Photospheric Emission in Fermi Gamma Ray Bursts
Medvedev M. V., Loeb A., 1999, ApJ, 526, 697
Mészáros P., 2006, Reports on Progress in Physics, 69, 2259
Mészáros P., Ramirez-Ruiz E., et al. 2002, ApJ, 578, 812
Mészáros P., Rees M. J., 2000, ApJ, 530, 292
Mizuta A., Ioka K., 2013a, ApJ, 777, 162
Mizuta A., Ioka K., 2013b, ApJ, 777, 162
Paczyński B., 1998, in Meegan C. A., Preece R. D., Koshut T. M., eds, Gamma-Ray Bursts, 4th Hunstville Symposium Vol. 428 of American Institute of Physics Conference Series, Gamma-ray bursts as hypernovae. pp 783–787
Panaitescu A., Mészáros P., 1998, ApJ, 492, 683
Pe'er A., 2008, ApJ, 682, 463
Pe'er A., Barlow H., O'Mahony S., et al. 2015, ArXiv e-prints
Pe'er A., Ryde F., 2011, ApJ, 732, 49
Pe'er A., Ryde F., et al. 2007, ApJL, 664, L1
Pe'er A., Waxman E., 2005, ApJ, 628, 857
Pe'er A., Zhang B., 2006, ApJ, 653, 454
Pe'Er A., Zhang B.-B., Ryde F., et al. 2012, MNRAS, 420, 468
Pilla R. P., Loeb A., 1998, ApJL, 494, L167
Preece R., Burgess J. M., von Kienlin A., et al. 2014, Science, 343, 51
Preece R. D., Briggs M. S., Mallozzi R. S., Pendleton G. N., Paciesas W. S., Band D. L., 1998, ApJL, 506, L23
Racusin J. L., Oates S. R., Schady P., Burrows D. N., de Pasquale M., Donato D., Gehrels N., Koch S., McEnery J., Piran T., Roming P., Sakamoto T., Swenson C., Troja E., Vasileiou V., Virgili F., Wanderman D., Zhang B., 2011, ApJ, 738, 138
Rees M. J., Mészáros P., 1994, ApJL, 430, L93
Rybicki G. B., Lightman A. P., 1986, Radiative Processes in Astrophysics. pp. 400. ISBN 0-471-82759-2. Wiley-VCH
Ryde F., 2004, ApJ, 614, 827
Ryde F., 2005, ApJ, 625, L95
Ryde F., Axelsson M., et al. 2010, ApJL, 709, L172
Ryde F., Pe'er A., 2009, ApJ, 702, 1211
Santana R., Barniol Duran R., Kumar P., 2014, ApJ, 785, 29
Sari R., Narayan R., Piran T., 1996, ApJ, 473, 204
Sari R., Piran T., Narayan R., 1998, ApJL, 497, L17
Scargle J. D., Norris J. P., Jackson B., Chiang J., 2013, ApJ, 764, 167
Shenoy A., Sonbas E., Dermer C., et al. 2013, ApJ, 778, 3
Spitkovsky A., 2008, ApJL, 682, L5
Tavani M., 1996, ApJ, 466, 768
Thompson C., Mészáros P., Rees M. J., 2007, ApJ, 666, 1012
Tierney D., von Kienlin A., 2011, GRB Coordinates Network, 12187, 1
Uhm Z. L., Zhang B., 2014, Nature Physics, 10, 351
van der Horst A. J., 2009, GRB Coordinates Network, 9691, 1
Wang X.-G., Zhang B., Liang E.-W., et al. 2015, ApJS, 219, 9
Wilson-Hodge C., Connaughton V., Longo F., Omodei N., 2008, GRB Coordinates Network, 8723, 1
Wilson-Hodge C. A., Foley S., 2010, GRB Coordinates Network, 10944, 1
Woosley S. E., Weaver T. A., 1995, ApJS, 101, 181
Wygoda N., Guetta D., Mandich M.-A., Waxman E., 2015, ArXiv e-prints
Yu H.-F., Greiner J., van Eerten H., et al. 2015, A&A, 573, A81
Zhang B., Pe'er A., 2009, ApJL, 700, L65
Zhang B., Yan H., 2011, ApJ, 726, 90
Zhang B.-B., Uhm Z. L., Connaughton V., et al. 2015, ArXiv e-prints
Zhang W., Woosley S. E., MacFadyen A. I., 2003, ApJ, 586, 356